Research Square

Preprints are preliminary reports that have not undergone peer review.
They should not be considered conclusive, used to inform clinical practice,
or referenced by the media as validated information.

Breaking Penalty Plateaus with Quantum-Inspired Improved Particle Swarm Optimization

Prashant Pandey

prashant.has.pandey@gmail.com

GLA University

Raju Prajapati

Amity University

Research Article

Keywords: quantum-inspired particle swarm optimization, improved particle swarm optimization, penalty method, constrained nonlinear programming, selected multimodal benchmark functions, bounded potential fields

Posted Date: August 12th, 2026

DOI: https://doi.org/10.21203/rs.3.rs-10655020/v1

License: This work is licensed under a Creative Commons Attribution 4.0 International License.
Read Full License

Additional Declarations: No competing interests reported.

Breaking Penalty Plateaus with Quantum-Inspired Improved Particle Swarm Optimization

Prashant Kumar Pandey [1*]

Raju Prajapati [2]

[1]Department of Mathematics, GLA University, Mathura, Uttar Pradesh, India

[2]Amity Institute of Applied Sciences, Amity University Jharkhand, Ranchi, Jharkhand, India

Corresponding author: Prashant Kumar Pandey, prashant.has.pandey@gmail.com

rprajapati@rnc.amity.edu

Abstract

This paper studies a quantum-inspired exploratory variant of improved particle swarm optimization (IPSO) for constrained nonlinear programs handled through a quadratic penalty formulation. The study is motivated by the broader view that PSO-type algorithms may benefit from quantum-inspired movement when classical velocity-based search loses exploratory strength on penalized landscapes with multiple local attraction regions. Instead of treating any particular improved PSO scheme as exceptional, the present work uses a representative IPSO baseline from the wider PSO class and replaces its velocity-driven movement with bounded-potential quantum displacement laws. The resulting quantum-inspired PSO (QIPSO) variants use Lorentz (LR), Rosen–Morse (RM), and Coulomb-like square-root (CS) potential fields to generate probability-controlled exploratory motion around the local attractor while retaining attraction toward personal and global best positions. Numerical experiments are performed on ten two-dimensional constrained benchmark functions using four penalty constants, $c \in \{10, 100, 1000, 10000\}$, with 30 independent replications for each algorithm–function–penalty setting. Across eleven improving function–penalty cases, all concentrated on the selected multimodal benchmarks, the best quantum variant reduces the mean absolute error of the IPSO baseline by approximately 42.24% to 99.96%. Feasible-trial rates are reported with these rows because some Rastrigin and Griewank improvements involve a strict-feasibility trade-off. The results also show that the classical IPSO baseline remains preferable on exploitation-dominant cases where it already reaches the known optimum to machine precision. This balanced behaviour indicates that quantum-inspired movement is particularly useful as a controlled nonlocal search mechanism for plateau-prone constrained multimodal landscapes, rather than as a universal replacement for all PSO searches.

Keywords: quantum-inspired particle swarm optimization; improved particle swarm optimization; penalty method; constrained nonlinear programming; selected multimodal benchmark functions; bounded potential fields.

1 Introduction

Constrained nonlinear programming problems (NLPPs) arise naturally in operations research, engineering design, and computational modelling. A widely used strategy for constrained

*Corresponding author.

NLPPs with inequalities is to transform the constrained problem into an unconstrained problem through a penalty function. Penalty-based and related constraint-handling techniques have been widely studied in evolutionary and nature-inspired optimization [7, 8]. Once this transformation is applied, the quality of the final solution depends not only on the penalty constant but also on the ability of the search algorithm to balance exploration and exploitation on the penalized landscape. In this paper, exploration means sampling that can move the swarm outside its current locally attractive neighbourhood or basin, whereas exploitation means refinement around already discovered high-quality personal or global best information.

Particle swarm optimization (PSO) and improved particle swarm optimization (IPSO) variants are attractive for such problems because they are simple, population based, and capable of exploiting information from both individual and collective search experience [3, 4]. Important improvements to classical PSO include inertia-weight and constriction-factor mechanisms that help control the balance between exploration and convergence [5, 6]. However, constrained multimodal penalty landscapes may still generate plateau-like convergence behaviour. In this article, a plateau refers to a sustained flattening of the convergence curve or repeated-trial error when particles remain near locally attractive feasible or nearly feasible regions instead of exploring other promising basins. This effect is expected mainly for multimodal functions, and the numerical evidence below identifies it most clearly for the constrained Rastrigin, Himmelblau, and Griewank cases.

Quantum-inspired PSO methods offer an alternative movement mechanism. Instead of relying only on velocity memory, the particle position can be updated through probability-controlled displacement around an attractor, following the broader quantum-behaved PSO idea [10]. This motivates the present work: if quantum-inspired displacement can strengthen exploration in PSO-type algorithms, then an improved PSO method used for penalty-based constrained optimization can also be modified in this direction.

The central novelty is therefore an exploration-oriented quantum-inspired variant of improved PSO for constrained NLPPs. The proposed method does not alter the constrained benchmark functions or the quadratic penalty formulation; instead, it changes how particles search the penalized landscape. In classical improved PSO, exploitation is supplied by attraction to personal and global best positions, while exploration depends mainly on inertia, velocity persistence, and stochastic variation in the attraction terms. Once velocities contract and best positions cluster around the same basin, the movement can become strongly local. In the proposed quantum-inspired PSO (QI-PSO), the attractor still supplies exploitation toward promising memory points, but the potential-induced displacement adds an explicit nonlocal exploratory sampling mechanism. This allows the swarm to sample wider regions of the search space and to traverse plateau regions more effectively in selected multimodal constrained problems.

The main contributions of this paper are:

- formulation of a quantum-exploratory IPSO family for penalty-based constrained NLPPs;
- replacement of a representative improved PSO velocity movement by Lorentz (LR), Rosen–Morse (RM), and Coulomb-like square-root (CS) quantum displacement mechanisms;
- comparative evaluation of IPSO and three bounded-potential QI-PSO variants under four penalty constants;
- identification of eleven MAE-improving function–penalty cases in the ten-function benchmark suite, with feasibility rates reported for the same cases;
- a standard-benchmark generalization evaluation showing that QI-PSO also improves the IPSO mean-objective error on non-overlapping unconstrained test functions;

- balanced analysis of cases where the classical IPSO baseline remains better because the search is already exploitation-dominant.

2 Literature Survey

2.1 Improved PSO for Penalty-Based Constrained Optimization

Constraint handling is a central issue in applying population-based search methods to constrained numerical optimization. General surveys by Coello Coello [7] and Mezura-Montes and Coello Coello [8] discuss penalty functions, feasibility rules, repair mechanisms, and other strategies for preserving useful search pressure in constrained spaces. In the PSO literature, penalty-based constrained optimization has also been studied directly; for example, Parsopoulos and Vrahatis [9] incorporated a nonstationary multistage penalty function into PSO for constrained benchmark problems.

Using a quadratic penalty formulation, Prajapati et al. [1] converted inequality-constrained benchmark functions into unconstrained penalized objectives. Their work used an improved PSO framework with a single-random-number velocity update, linearly decreasing inertia, constriction factor, and boundary control, and examined how different penalty constants affect the obtained solutions. In the present article, this work is used as a representative IPSO setting within the broader class of PSO algorithms for constrained optimization.

This interpretation is important for the positioning of the present study. The objective is not to present one IPSO variant as uniquely privileged, but to use it as a clear and reproducible PSO-class baseline. Since the limitation being studied is the possible stagnation of velocity-based PSO movement on selected multimodal penalized landscapes, the proposed modification is intended to show how quantum-inspired movement can improve exploration in this class of algorithms.

2.2 Quantum-Inspired PSO with Bounded Potential Fields

Quantum-inspired PSO methods replace the explicit velocity trajectory of classical PSO with probabilistic movement around an attractor. Sun, Feng, and Xu [10] introduced a quantum-behaved PSO model in which particle motion is described through a quantum delta-potential-well interpretation rather than a classical velocity trajectory. Related QPSO studies have examined global-search strategies, individual-particle behaviour and parameter selection, and nonlinear programming applications [11, 12, 13]. Alvarez-Alvarado et al. [2] later proposed three quantum-inspired swarm optimization algorithms using bounded potential fields. The present study considers the Lorentz (LR), Rosen–Morse (RM), and Coulomb-like square-root (CS) forms. These potential fields generate different displacement laws and therefore provide different search patterns around promising regions of the search space.

The scientific motivation for using such potential fields is that a quantum particle in a bound state is not assigned a single deterministic path. Instead, its possible location is described by a wavefunction, and the squared modulus of that wavefunction gives a probability density [14]. In a quantum-inspired optimizer, this idea is used as an analogy: the swarm attractor plays the role of the centre of a potential well, and the wavefunction-derived density becomes a sampling rule for the next displacement. Hence the potential field is not introduced as a claim about quantum-computing hardware; it is a principled way of replacing deterministic velocity propagation by a probability law whose local concentration and tail behaviour can be controlled.

This distinction is important for the present constrained optimization setting. A density concentrated near the attractor supports intensive search around a promising basin, while a density

with a non-negligible tail allows occasional movement away from that basin. In the terminology used in this article, the former contributes to local exploitation and the latter to broader exploration. The Lorentz, Rosen–Morse, and Coulomb-like square-root fields are therefore useful because they lead to closed-form displacement laws with different tail decay rates, giving a physically motivated family of stochastic search kernels rather than an arbitrary random perturbation.

The study of Alvarez-Alvarado et al. [2] is especially relevant here because it provides a systematic source for the bounded-potential quantum displacement laws adopted in this article. The present study does not simply compare two unrelated algorithms; it connects the penalty-based IPSO setting of Prajapati et al. [1] with the bounded-potential quantum movement mechanisms of Alvarez-Alvarado et al. [2]. This connection leads to the proposed QI-PSO-LR, QI-PSO-RM, and QI-PSO-CS variants.

3 Methodology

Guided by the two lines of work discussed above, the methodology keeps the constrained penalty formulation and the representative improved PSO search structure from Prajapati et al. [1], while replacing the velocity-based movement step with the bounded-potential quantum displacement laws reported by Alvarez-Alvarado et al. [2]. Thus, the baseline remains a member of the PSO family, and the proposed variants test the broader hypothesis that quantum-inspired movement can improve the exploratory behaviour of PSO-type algorithms on plateau-prone constrained landscapes.

Consider the constrained NLPP

$$\min_{x\in X} f(x), \qquad g_j(x) \le 0, \quad j = 1, 2, \ldots, m. \tag{1}$$

Here $x = (x_1, \ldots, x_d)$ is the decision vector, $X \subset \mathbb{R}^d$ is the bounded search domain, $f : X \to \mathbb{R}$ is the objective function, and $g_j : X \to \mathbb{R}$ are inequality constraint functions. The benchmark functions used in this study are two-dimensional, so $d = 2$ in the numerical experiments. In the algorithmic notation below, $i = 1, \ldots, N$ indexes particles, $j = 1, \ldots, d$ indexes coordinates, and t indexes iterations. Using the quadratic penalty approach, the constrained problem is transformed into the unconstrained penalized objective

$$F_c(x) = f(x) + c\sum_{j=1}^{m} \max\{0, g_j(x)\}^2, \tag{2}$$

where $c > 0$ is the penalty constant. Larger values of c impose stronger cost on infeasible points, while smaller values permit broader movement near the feasible boundary. Throughout this paper, the penalty landscape means the objective surface of F_c, the unconstrained problem induced by applying the quadratic penalty transformation to the constrained NLPP. Thus, statements about flat regions, basins, or plateaus refer to the geometry of this penalized objective for a specified value of c.

3.1 Improved PSO Baseline

The baseline IPSO updates particle velocity according to

$$v_i^{t+1} = \chi\left[w_t v_i^t + c_1 r_i^t (p_i^t - x_i^t) + c_2(1 - r_i^t)(\widetilde{g}_i^t - x_i^t)\right], \tag{3}$$

where x_i^t and v_i^t are the position and velocity of particle i, p_i^t is its personal best position, $\widetilde{g}_i^t = (\widetilde{g}_{i1}^t, \ldots, \widetilde{g}_{id}^t)$ is the current swarm-level global best available immediately before particle i

is moved in iteration t, $r_i^t \sim U(0,1)$ is sampled once for that particle update, $c_1 = c_2 = 2$, and $\chi = 0.73$. If $T_{\max}$ is the iteration budget, the linearly decreasing inertia weight is

$$w_t = w_{\max} - \frac{t}{T_{\max} - 1}(w_{\max} - w_{\min}), \qquad w_{\max} = 0.9, \quad w_{\min} = 0.4,$$

for $t = 0, 1, \ldots, T_{\max} - 1$. The baseline implementation updates particles sequentially. After particle i is moved and evaluated under F_c, its personal best is updated if the new position is better; if this also improves the swarm best, the global best is updated immediately and can influence the next particle in the same iteration. Equivalently, if $\widehat{p}_i^{t+1}$ denotes the candidate personal best after particle i has been evaluated, define the available personal-best set

$$\mathcal{P}_i^t = \{\widehat{p}_k^{t+1} : 1 \le k \le i\} \cup \{p_k^t : i < k \le N\}.$$

The running global best is then selected as

$$\widetilde{g}_{i+1}^t \in \arg\min_{y \in \mathcal{P}_i^t} F_c(y).$$

At the end of the iteration, this running best becomes g^{t+1}. The position is updated as

$$x_i^{t+1} = x_i^t + v_i^{t+1}, \tag{4}$$

with boundary control applied componentwise.

This IPSO form differs from the standard PSO update mainly through the use of the constriction factor and a single scalar random number that couples the cognitive and social pulls. The decreasing inertia weight permits broader movement in the early iterations and favours local refinement later, while the constriction factor prevents excessive velocity growth. These features make the method a suitable baseline for penalty-based constrained optimization because it combines directional memory with controlled attraction toward the best positions already discovered.

At the same time, this velocity-driven structure can become conservative once the swarm has clustered near a locally attractive feasible or nearly feasible region. When the penalty landscape contains flat regions or multiple basins, small velocities and repeated attraction to the same personal and global best positions may reduce the probability of escaping that neighbourhood. This motivates replacing the velocity step, rather than the penalty formulation or the benchmark functions, with a quantum-inspired displacement mechanism.

3.2 Quantum Potential-Well Motivation

The quantum terminology used in this paper follows the standard potential-well interpretation adopted in quantum-behaved PSO. In one spatial coordinate z, a bound quantum state is represented by a wavefunction $\psi(z)$, and the probability of observing the particle in a region is determined by the density

$$p_\psi(z) = |\psi(z)|^2, \qquad \int_{-\infty}^{\infty} p_\psi(z)\, dz = 1. \tag{5}$$

For a time-independent potential $V(z)$, the corresponding stationary wavefunction satisfies

$$-\frac{\hbar^2}{2m_q}\frac{d^2\psi(z)}{dz^2} + V(z)\psi(z) = E\psi(z), \tag{6}$$

where m_q denotes a physical particle mass, E is the energy level, and $\hbar$ is the reduced Planck constant. In the optimization algorithm these physical constants are not used as numerical

parameters. Instead, after nondimensionalization, the analytic form of the wave function is used only to obtain a probability distribution for a signed displacement from the attractor.

This leads to the following optimization interpretation. The local attractor is the center of the potential well; the adaptive length scale $|x_{ij}^t - m_j^t|$ plays the role of the well width; and a random number $u \sim U(0,1)$ represents the sampling variable used to draw a displacement from the potential-induced density. Thus, the quantum potential supplies a stochastic search kernel. It keeps the particle probabilistically localized around the attractor, but it does not force all future positions to remain close to it. The tail of the density determines how often larger jumps can occur.

The three bounded-potential fields considered in this study are scientifically motivated because their stationary models yield simple closed-form sampling laws [2]. The Lorentz field produces a comparatively heavy algebraic tail, the Rosen-Morse field gives a hyperbolic-secant type tail, and the Coulomb-like square-root field gives a stretched-exponential tail. These differences are directly relevant to the hypothesis of this work: when the penalized objective creates separated attraction basins or plateau-like regions, a potential-induced sampling law can preserve nonzero probability of testing points outside the currently clustered swarm neighbourhood.

Figure 1 visualizes this mechanism in normalized coordinates. The left panel shows the attractor-centred potential wells, and the right panel shows the probability that the dimensionless quantum displacement exceeds a prescribed escape radius. The plot clarifies the algorithmic role of the potential fields: they are not additional objective functions, but search kernels that control localization near the attractor and occasional nonlocal movement.

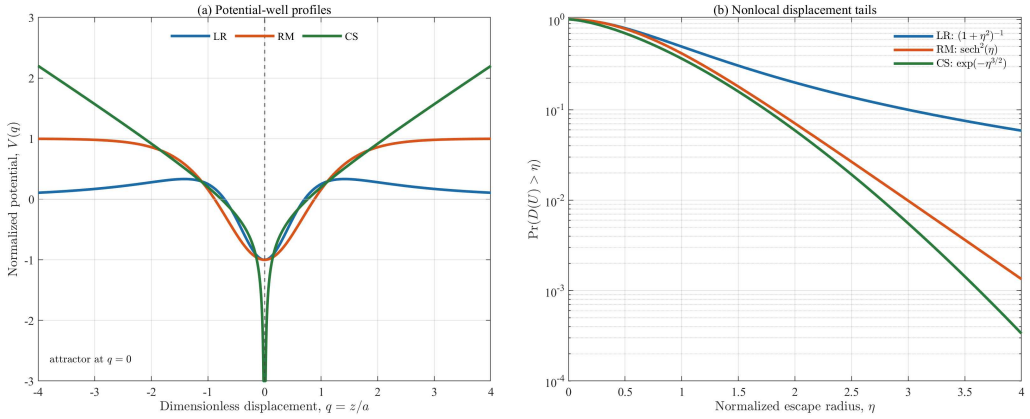

Figure 1: Potential-well mechanism used in QI-PSO. The potentials are plotted as $\widetilde{V}(q) = (2m_q a^2/\hbar^2)V(z)$ with $q = z/a$, where a is the well-width scale; the Coulomb-like square-root (CS) well is clipped near $q = 0$ for visibility.

3.3 Quantum-Inspired PSO

In QI-PSO, a particle is not described by a deterministic velocity trajectory. Instead, its next position is sampled from the potential-well probability mechanism described above. The attractor represents the combined influence of the particle's personal best and the swarm's global best, while the potential-induced probability law controls how far the particle may move away from this attractor. Thus, the quantum potential well replaces the classical velocity-memory mechanism by a stochastic localization mechanism. Accordingly, the proposed QI-PSO variants do not initialize, store, or update a velocity vector; the particle state is advanced directly by the sampled attractor-displacement rule.

The choice of potential function is important because it determines the spread and tail be-

haviour of the displacement distribution. A more localized potential concentrates samples near the attractor and therefore favours exploitation, whereas a heavier-tailed potential increases the chance of nonlocal exploratory jumps. In the present QI-PSO variants, Lorentz (LR), Rosen–Morse (RM), and Coulomb-like square-root (CS) potential fields are used to generate different quantum displacement laws. These laws preserve attraction toward promising regions while allowing probabilistic movement across plateau-like or multimodal regions of the penalized search landscape.

In the proposed QI-PSO variants, the attractor structure of the baseline method is retained but the velocity step is replaced. Let $x_i^t = (x_{i1}^t, \ldots, x_{id}^t)$ be the position of particle i at iteration t, and let $g^t = (g_1^t, \ldots, g_d^t)$ be the swarm best used by the QI-PSO update at that iteration. A scalar particle-level mixing draw is used for the attractor, but it is denoted separately from the IPSO velocity random number: $\lambda_i^t \sim U(0,1)$ is sampled once for particle i and is shared across all coordinates. This λ_i^t is a fresh QI-PSO mixing draw for forming the attractor, not the r_i^t used in Eq. (3). For coordinate j, define

$$a_{ij}^t = \frac{c_1 \lambda_i^t p_{ij}^t + c_2(1-\lambda_i^t) g_j^t}{c_1 \lambda_i^t + c_2(1-\lambda_i^t) + \epsilon}, \tag{7}$$

where $\epsilon > 0$ is a small numerical stabilizer, implemented as machine epsilon in the scripts, and is retained for robustness if general coefficient choices are used. With the present $c_1 = c_2 = 2$, the denominator is positive even without this term. Thus λ_i^t controls the particle-level balance between the personal-best component and the swarm-best component in the attractor; it is not the quantum displacement draw. Let

$$m_j^t = \frac{1}{N} \sum_{i=1}^{N} p_{ij}^t \tag{8}$$

be the jth component of the mean personal best of the swarm. The quantum-inspired position update is applied component-wise:

$$x_{ij}^{t+1} = a_{ij}^t + s_{ij}^t |x_{ij}^t - m_j^t| D(u_{ij}^t), \tag{9}$$

where $s_{ij}^t \in \{-1, +1\}$ is an independently sampled coordinate direction with equal probabilities and $u_{ij}^t \sim U(0,1)$ is sampled independently for each coordinate. The displacement functions are not arbitrary perturbation terms. Following the bounded-potential construction in [2], they are obtained by solving the stationary potential-well models for the Lorentz (LR), Rosen–Morse (RM), and Coulomb-like square-root (CS) fields, normalizing the corresponding probability density, and using $u \sim U(0,1)$ to sample the dimensionless displacement. If z is the sampled physical displacement and a is the potential-well width, then z/a gives the factor $D(u)$ used in Eq. (9). For $u \in (0,1)$, the selected potential field therefore determines $D(u)$ as follows:

$$D_{\mathrm{LR}}(u) = \sqrt{\frac{1-u}{u}}, \tag{10}$$

$$D_{\mathrm{RM}}(u) = \operatorname{arcosh}\left(\frac{1}{\sqrt{u}}\right), \tag{11}$$

$$D_{\mathrm{CS}}(u) = \left[\log\left(\frac{1}{u}\right)\right]^{2/3}. \tag{12}$$

These are nonnegative dimensionless displacement magnitudes; the sign of the coordinate move is supplied separately by s_{ij}^t. Here arcosh is the inverse hyperbolic cosine.

Equation (9) is the key algorithmic modification. In the baseline IPSO, a particle may continue to follow a small velocity pattern once the swarm has gathered around a local region. In QI-PSO, the quantum displacement $D(u)$ keeps the next move probabilistic even after the local

attractor has been formed. The Lorentz (LR), Rosen–Morse (RM), and Coulomb-like square-root (CS) potential fields therefore act as exploration-localization controllers: the tail controls the probability of exploratory departures from the attractor, while the concentration near the attractor controls local search intensity.

For clarity, Algorithm 1 summarizes the implemented QI-PSO variant. The pseudocode highlights the distinctive point that the IPSO velocity update is not modified; it is removed and replaced by direct probabilistic sampling around the local attractor.

Algorithm 1. Velocity-free bounded-potential QI-PSO

Input: penalized objective F_c, bounds X, population size N, dimension d, iteration budget $T_{\max}$, coefficients $c_1 = c_2 = 2$, and potential type LR (Lorentz), RM (Rosen–Morse), or CS (Coulomb-like square-root).
Output: final best position $g^{T_{\max}}$ and objective value $F_c(g^{T_{\max}})$.

1. Initialize $x_i^0 \in X$ randomly for $i = 1, \ldots, N$; set $p_i^0 = x_i^0$.
2. Evaluate $F_c(p_i^0)$ and set $g^0 \in \arg\min_{1 \le i \le N} F_c(p_i^0)$.
3. For $t = 0, 1, \ldots, T_{\max} - 1$, compute $m_j^t = N^{-1} \sum_{i=1}^{N} p_{ij}^t$ for $j = 1, \ldots, d$.
4. For each particle i, draw one particle-level attractor variable $\lambda_i^t \sim U(0, 1)$.
5. Form the coordinate attractors a_{ij}^t from Eq. (7) using p_i^t and the current swarm best g^t.
6. For each coordinate j, draw $u_{ij}^t \sim U(0, 1)$ and $s_{ij}^t \in \{-1, +1\}$ with equal probabilities.
7. Select $D = D_{\mathrm{LR}}$ (Lorentz), D_{RM} (Rosen–Morse), or D_{CS} (Coulomb-like square-root) according to the chosen potential field, and update x_{ij}^{t+1} by Eq. (9).
8. Apply boundary control component-wise, evaluate $F_c(x_i^{t+1})$, and replace p_i^t by x_i^{t+1} if the new point is better.
9. After all particles have been evaluated, set $g^{t+1} \in \arg\min_{1 \le i \le N} F_c(p_i^{t+1})$.
10. Stop after $T_{\max}$ iterations and return $g^{T_{\max}}$.

Velocity-free feature: no velocity vector v_i^t is initialized, stored, or updated in Steps 3–10.

The three displacement laws have different tail behaviours. The following probabilities follow by direct inversion of the bounded-potential sampling laws in [2]. For $U \sim U(0, 1)$ and $\eta > 0$, with sech denoting the hyperbolic secant,

$$\Pr(D_{\mathrm{LR}}(U) > \eta) = \frac{1}{1 + \eta^2}, \tag{13}$$

$$\Pr(D_{\mathrm{RM}}(U) > \eta) = \operatorname{sech}^2(\eta), \tag{14}$$

$$\Pr(D_{\mathrm{CS}}(U) > \eta) = \exp(-\eta^{3/2}). \tag{15}$$

Thus rare large moves remain possible, but their frequency depends on the selected potential field. The adaptive multiplier $|x_{ij}^t - m_j^t|$ contracts the move size when the personal bests have clustered and expands it when the particle is far from the swarm's mean memory. This gives a simple exploration–exploitation interpretation: the attractor keeps the search exploitatively oriented toward good regions, while the component-wise quantum displacement supplies controlled nonlocal exploratory sampling that can help traverse penalty plateaus in multimodal constrained landscapes.

3.4 Theoretical Exploration Interpretation

The exploration effect of QI-PSO can be formalized through a one-step nonlocal-sampling probability. The proposition below is the authors' one-step comparison derived from Eqs. (3) and (9); the broader probability-controlled-attractor idea is motivated by the QPSO literature cited above. This does not prove universal superiority in objective value, but it shows that the proposed quantum update preserves a probabilistic tail around the attractor when the classical

velocity update is locally bounded. The two events below are centered differently because the classical update is naturally measured from the current particle position, whereas the quantum update is sampled around the attractor a_{ij}^t. Therefore, the proposition should be read as an exploration mechanism statement, not as a full global convergence theorem.

Proposition. Consider a single coordinate j of particle i at iteration t. Suppose that the classical IPSO swarm is locally clustered in the sense that

$$|p_{ij}^t - x_{ij}^t| \le \delta, \qquad |\widetilde{g}_{ij}^t - x_{ij}^t| \le \delta, \qquad |v_{ij}^t| \le \nu,$$

for some $\delta, \nu \ge 0$. Then the one-step classical IPSO displacement satisfies

$$|x_{ij}^{t+1} - x_{ij}^t| \le \chi\left(w_t\nu + (c_1 + c_2)\delta\right).$$

Consequently, for any escape radius

$$\rho > \chi\left(w_t\nu + (c_1 + c_2)\delta\right),$$

the classical IPSO escape probability is zero:

$$\Pr\left(|x_{ij}^{t+1} - x_{ij}^t| > \rho\right) = 0.$$

For QI-PSO, let

$$L_{ij}^t = |x_{ij}^t - m_j^t|.$$

If $L_{ij}^t > 0$, then for every finite $\rho > 0$,

$$\Pr\left(|x_{ij}^{t+1} - a_{ij}^t| > \rho\right) > 0$$

for each of the Lorentz, Rosen–Morse, and Coulomb-like square-root potential fields.

Proof. From the classical IPSO velocity update in Eq. (3),

$$\begin{aligned} |v_{ij}^{t+1}| &= \chi\left|w_t v_{ij}^t + c_1 r_i^t (p_{ij}^t - x_{ij}^t) + c_2(1 - r_i^t)(\widetilde{g}_{ij}^t - x_{ij}^t)\right| \\ &\le \chi\left[w_t|v_{ij}^t| + c_1 r_i^t |p_{ij}^t - x_{ij}^t| + c_2(1 - r_i^t)|\widetilde{g}_{ij}^t - x_{ij}^t|\right] \\ &\le \chi\left(w_t\nu + (c_1 + c_2)\delta\right), \end{aligned} \tag{16}$$

because $0 \le r_i^t \le 1$. Since $x_{ij}^{t+1} - x_{ij}^t = v_{ij}^{t+1}$, the stated bound follows immediately. Hence any escape radius larger than this upper bound cannot be crossed by the classical IPSO particle in one step, giving escape probability zero. In particular, because $\chi = 0.73$ and $0.4 \le w_t \le 0.9$, the inertial part is strictly contractive, since $\chi w_t < 1$.

For QI-PSO, Eq. (9) gives

$$|x_{ij}^{t+1} - a_{ij}^t| = L_{ij}^t D(U),$$

where $U \sim U(0,1)$ is the coordinate-level displacement draw and D denotes one of the three displacement laws above. Thus

$$\Pr\left(|x_{ij}^{t+1} - a_{ij}^t| > \rho\right) = \Pr\left(D(U) > \frac{\rho}{L_{ij}^t}\right).$$

Using the displacement laws of the three potential fields,

$$\Pr_{\mathrm{LR}}\left(|x_{ij}^{t+1} - a_{ij}^t| > \rho\right) = \frac{1}{1 + (\rho/L_{ij}^t)^2}, \tag{17}$$

$$\Pr_{\mathrm{RM}}\left(|x_{ij}^{t+1} - a_{ij}^t| > \rho\right) = \operatorname{sech}^2(\rho/L_{ij}^t), \tag{18}$$

$$\Pr_{\mathrm{CS}}\left(|x_{ij}^{t+1} - a_{ij}^t| > \rho\right) = \exp\left[-(\rho/L_{ij}^t)^{3/2}\right]. \tag{19}$$

All three quantities are strictly positive for finite ρ whenever $L_{ij}^t > 0$. Therefore, under this one-step metric, QI-PSO retains a nonzero probability of leaving any finite attractor neighbourhood, whereas locally clustered classical IPSO has a bounded current-position step and may have zero probability of crossing a larger one-step radius. This proves the claimed exploration mechanism in the stated probabilistic sense. The result should be interpreted as an attractor-neighbourhood sampling guarantee, not as a global convergence or universal performance guarantee.

4 Benchmark Functions

Table 1 lists the constrained benchmark functions considered in the numerical study. Each function is two-dimensional, and the constraints are chosen such that the known optimum of the corresponding unconstrained benchmark remains feasible. The full suite includes both multimodal and exploitation-dominant landscapes; the plateau-related claim is not made for every function, but is evaluated on the selected multimodal cases where the results show persistent IPSO error.

Table 1: Constrained benchmark functions and domains.

Function	**Name**	**Domain**	$f_{\min}$ **at** x^*	**Constraint(s)**
f_1	Rosenbrock	$[-2.048, 2.048]^2$	0 at $(1,1)$	$x_1^2 + x_2^2 \leq x_1 + x_2$
f_2	Rastrigin	$[-5.12, 5.12]^2$	0 at $(0,0)$	$x_1 x_2 \leq 0$
f_3	Fletcher	$[-5,5]^2$	0 at $(-1,-1)$	$x_1^2 + x_2^2 \leq 2,\ x_1 \leq x_2$
f_4	Leon	$[-1.2, 1.2]^2$	0 at $(1,1)$	$x_1^2 + x_2^2 \leq x_1 + x_2$
f_5	Himmelblau	$[-6,6]^2$	0 at $(3,2)$	$x_2^2 + 5 \leq x_1^2$
f_6	Griewank	$[-10,10]^2$	0 at $(0,0)$	$x_1 x_2 \geq 0$
f_7	Trid	$[-4,4]^2$	-2 at $(2,2)$	$x_1^2 + x_2^2 \leq 8$
f_8	Booth	$[-10,10]^2$	0 at $(1,3)$	$3x_1 \leq x_2,\ x_1^2 + x_2^2 \leq 10$
f_9	Matyas	$[-10,10]^2$	0 at $(0,0)$	$x_1 x_2 \leq 0$
f_{10}	Liarwhd	$[-5,5]^2$	0 at $(1,1)$	$x_1 + x_2 \leq 2$

For the selected multimodal functions, Fig. 2 uses top-view contour maps because they make the constraint geometry, feasible sectors, and multiple local attraction regions visible on the same plane. This view is more useful for the present constrained optimization discussion than a three-dimensional surface plot, where the constraint boundary and feasible region can be visually obscured.

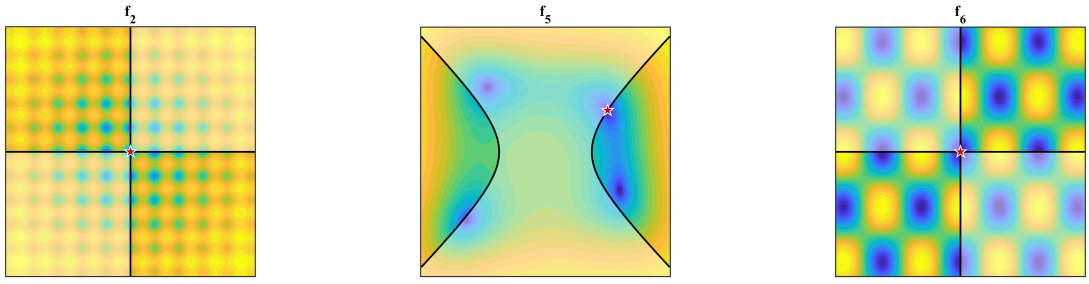

(a) f_2 Rastrigin **(b)** f_5 Himmelblau **(c)** f_6 Griewank

Figure 2: Constraint-aware contour maps for selected constrained functions in Table 1; black curves denote active constraints, and stars mark known feasible optima.

The corresponding surface morphology in Fig. 3 highlights the ruggedness and separated basin structure of these constrained multimodal landscapes.

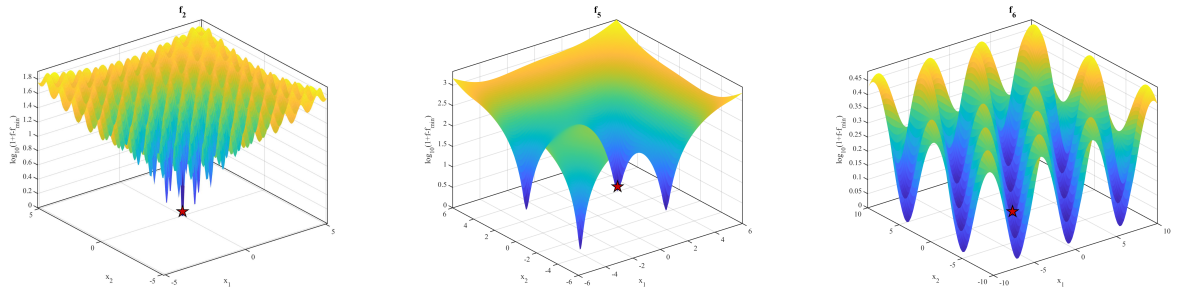

(a) f_2 Rastrigin **(b)** f_5 Himmelblau **(c)** f_6 Griewank

Figure 3: Surface plots for selected constrained functions in Table 1, showing the rugged basins that motivate nonlocal QI-PSO movement.

5 Experimental Design

The numerical comparison includes the baseline IPSO and the three quantum-inspired variants QI-PSO-LR, QI-PSO-RM, and QI-PSO-CS, where LR, RM, and CS denote the Lorentz, Rosen–Morse, and Coulomb-like square-root potential fields, respectively. Four penalty constants are considered: $c = 10$, 100, 1000, and 10000. For each algorithm–function–penalty combination, 30 independent replications are performed with a population size of 50 and a maximum of 100 iterations. Thus, the constrained comparison contains 40 function–penalty cases and 4800 individual algorithm runs across the four algorithms. A solution is regarded as feasible when the maximum positive constraint violation is not greater than 10^{-6}.

To support reproducibility, all stochastic trials were generated from a fixed random-seed protocol indexed by function, penalty constant, algorithm, and trial number. For the constrained suite, the master seed was 2025 and the run seed was

$$2025 + 100000\,\kappa_f + 10000\,\kappa_c + 1000\,\kappa_a + \ell,$$

where κ_f, κ_c, κ_a, and ℓ denote the deterministic integer labels for the function, penalty constant, algorithm, and replication, respectively. The replication label ℓ is distinct from the IPSO random draw r_i^t in Eq. (3). The QI-PSO variants use the separate scalar particle-level mixing draw λ_i^t to form the attractor in Eq. (7); the quantum direction s_{ij}^t and displacement variable u_{ij}^t are sampled component-wise as in Eq. (9). The numerical settings and tabulated data are retained to support verification of the reported results.

The primary error measure is the mean absolute error

$$\mathrm{MAE} = \frac{1}{R}\sum_{\ell=1}^{R}\left|f(x_\ell^{best}) - f_{\min}\right|, \tag{20}$$

where $R = 30$, x_ℓ^{best} is the best solution obtained in replication ℓ, and $f_{\min}$ is the known reference optimum value. The percentage reduction of a quantum variant over the IPSO baseline is computed as

$$\Delta(\%) = 100\frac{\mathrm{MAE}_{\mathrm{IPSO}} - \mathrm{MAE}_{\mathrm{QI}}}{\mathrm{MAE}_{\mathrm{IPSO}}}. \tag{21}$$

where $\mathrm{MAE}_{\mathrm{QI}}$ denotes the MAE of the QI-PSO variant being compared. This percentage is reported only for cases where the IPSO MAE is positive and the best quantum variant gives a smaller MAE; cases where IPSO already reaches machine precision are discussed separately.

6 Exploration, Convergence, and Error Results

The results show two distinct patterns. First, on the selected plateau-prone constrained multimodal cases shown in Fig. 2, the quantum variants improve exploratory reach and reduce the repeated-trial mean error of the IPSO baseline. Second, on several relatively easy or exploitation-dominant constrained functions, the IPSO baseline reaches the known optimum to machine precision. In these cases, the quantum variants should not be interpreted as superior. Presenting both patterns is important: it shows that QI-PSO is not merely a numerical replacement for IPSO, but an exploration-oriented modification whose advantage appears when the penalized landscape contains multimodal traps or plateau-like convergence.

From an exploration point of view, the key observation is that the quantum variants continue to sample around the local attractor through a probability distribution rather than through a decaying velocity trajectory. This added nonlocal sampling is useful when the IPSO curve has flattened because the swarm is locally exploiting the same attraction region. The resulting convergence curves show lower sustained error levels on the selected multimodal functions. Thus, the novelty is reflected not only in final objective values but also in convergence behaviour: QI-PSO is better able to soften the plateau observed in the baseline IPSO.

All four algorithms are evaluated on every function–penalty case. Figure 4 and Table 2 are filtered summaries: they report only those cases where at least one QI-PSO variant gives a lower MAE than IPSO, while the complementary IPSO-favourable cases are reported separately in Table 3.

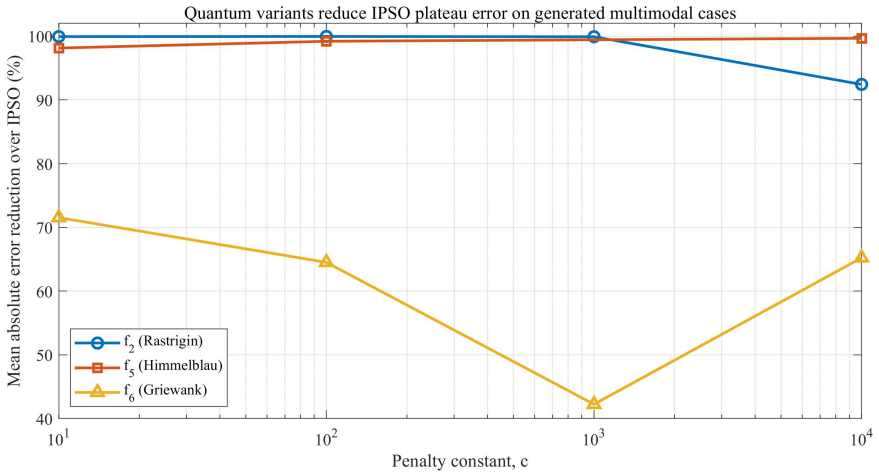

Figure 4: Best QI-PSO error reduction over IPSO for the improving constrained cases listed in Table 2.

The best QI-PSO variant in Table 2 is selected by MAE reduction, not by feasibility rate. The feasibility columns therefore qualify the interpretation of the improvement: the Himmelblau rows improve both objective accuracy and feasibility rate, while several Rastrigin and Griewank rows reduce MAE with lower feasible-trial rates than IPSO. The saved result table also records mean maximum constraint violations; for the best QI-PSO variants in the eleven rows these range from 0 to 2.71×10^{-4}. Thus the central constrained claim should be read as an improvement in objective-error behaviour on plateau-prone penalized landscapes, with feasibility reported separately rather than assumed from MAE alone.

Table 2 indicates that bounded-potential movement is most useful when the constrained landscape is multimodal and the repeated-trial mean error of IPSO remains nonzero. Since each of the ten benchmark functions is evaluated under four penalty constants, the experimental suite contains forty function–penalty combinations. Table 2 reports all eleven combinations in

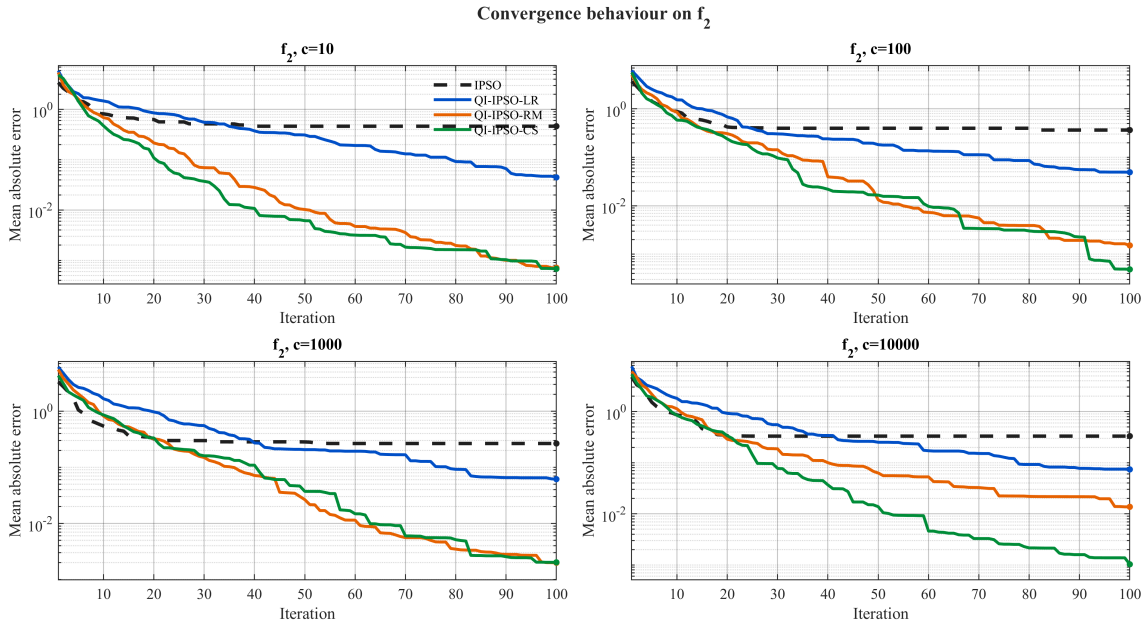

Figure 5: Mean convergence for constrained f_2 (Rastrigin), corresponding to the improving cases in Table 2.

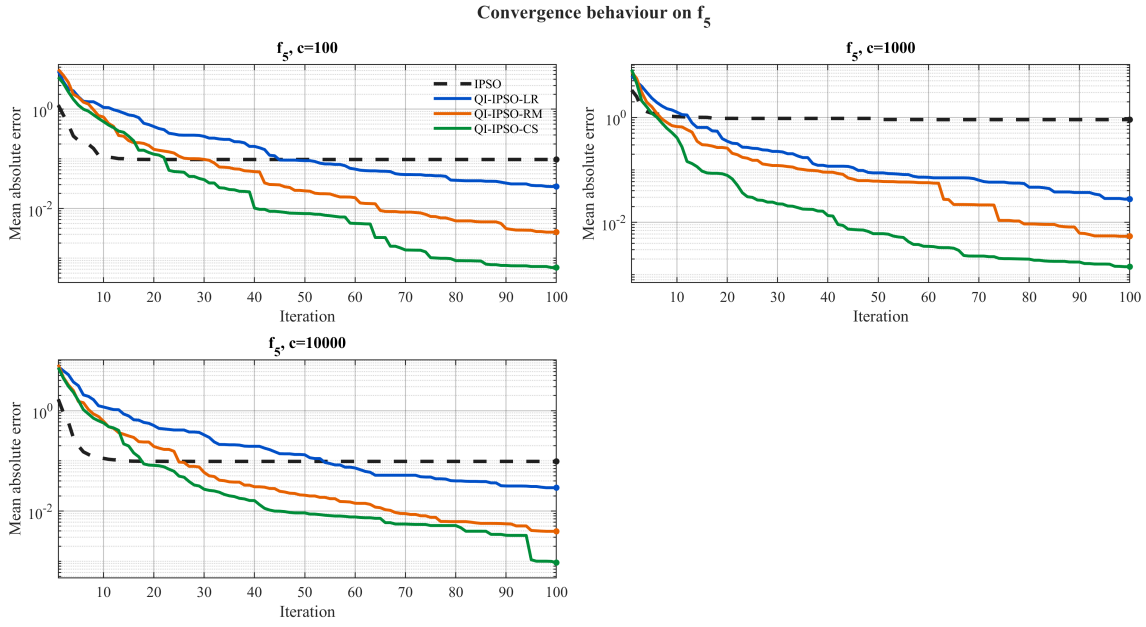

Figure 6: Mean convergence for constrained f_5 (Himmelblau).

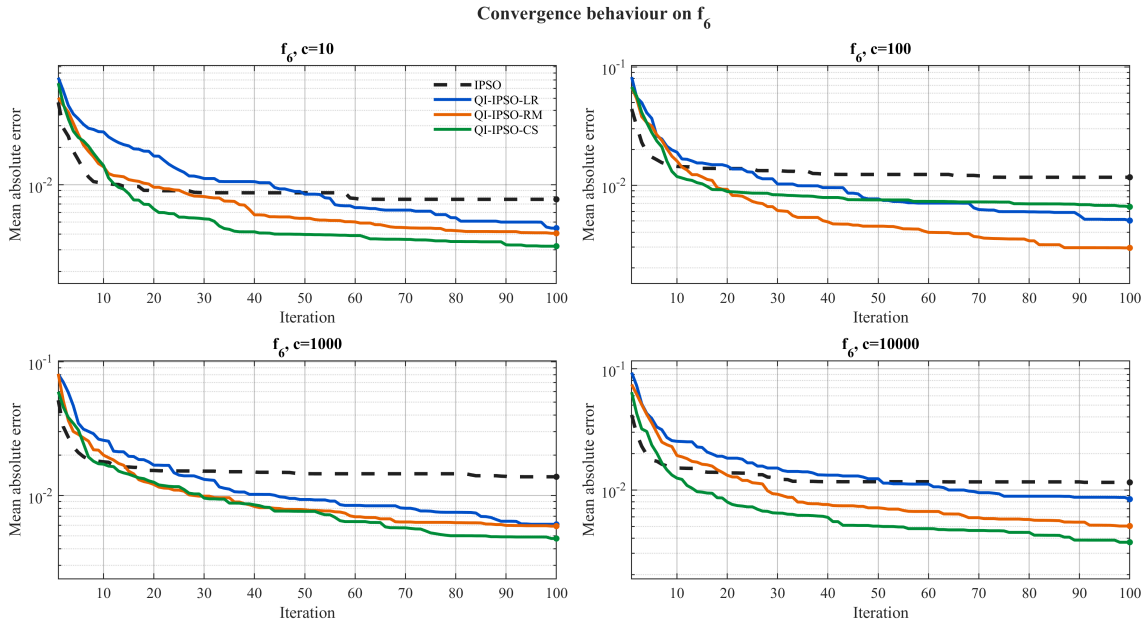

Figure 7: Mean convergence for constrained f_6 (Griewank), corresponding to the improving cases in Table 2.

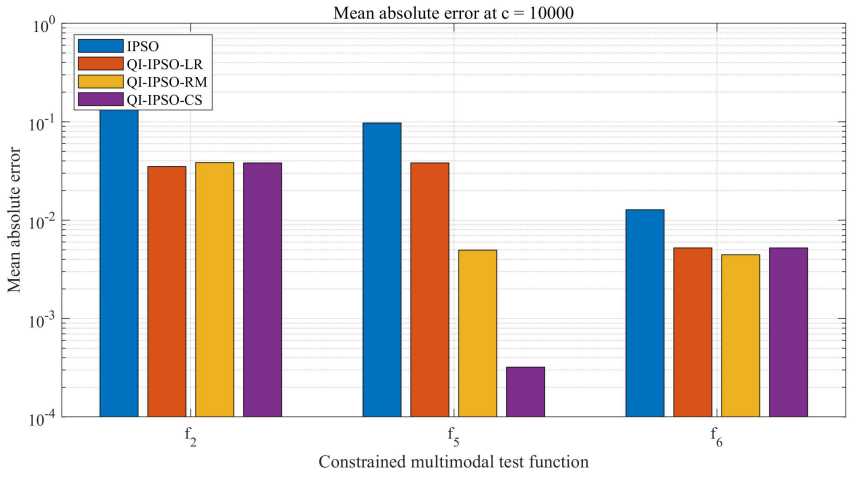

Figure 8: Mean absolute error at $c = 10000$ for selected constrained functions in Table 1; lower bars indicate better accuracy.

Table 2: Eleven improving function–penalty cases from the selected multimodal benchmarks. LR, RM, and CS denote the Lorentz, Rosen–Morse, and Coulomb-like square-root potential-field variants, respectively. Feasibility rates are proportions of the 30 trials satisfying the 10^{-6} maximum-violation tolerance.

Function	c	IPSO MAE	Best QI-PSO	QI-PSO MAE	Reduction (%)	IPSO feas.	QI feas.
f_2	10	2.6532×10^{-1}	CS	1.7236×10^{-4}	99.94	1.00	0.93
f_2	100	5.3064×10^{-1}	CS	2.1953×10^{-4}	99.96	1.00	0.90
f_2	1000	4.3115×10^{-1}	CS	3.8104×10^{-4}	99.91	1.00	0.97
f_2	10000	4.6431×10^{-1}	LR	3.5144×10^{-2}	92.43	1.00	0.43
f_5	10	8.5862×10^{-2}	CS	1.6010×10^{-3}	98.14	0.93	0.97
f_5	100	1.4429×10^{-1}	CS	1.1524×10^{-3}	99.20	0.90	1.00
f_5	10000	9.7442×10^{-2}	CS	3.2038×10^{-4}	99.67	0.93	1.00
f_6	10	1.1114×10^{-2}	RM	3.1628×10^{-3}	71.54	1.00	0.80
f_6	100	1.0767×10^{-2}	CS	3.8208×10^{-3}	64.51	1.00	0.83
f_6	1000	9.3696×10^{-3}	RM	5.4116×10^{-3}	42.24	1.00	0.70
f_6	10000	1.2822×10^{-2}	RM	4.4580×10^{-3}	65.23	0.97	0.93

Table 3: Representative IPSO-favourable cases at $c = 10000$. In the best QI-PSO result column, LR, RM, and CS denote the Lorentz, Rosen–Morse, and Coulomb-like square-root variants, respectively.

Func.	Name	IPSO MAE	Best QI	Explanation
f_1	Rosenbrock	1.36×10^{-31}	CS: 1.22×10^{-4}	The optimum is reached by IPSO; additional nonlocal sampling leaves a small residual error.
f_3	Fletcher	2.83×10^{-10}	CS: 2.25×10^{-4}	IPSO has enough exploitation pressure for this constrained surface.
f_4	Leon	3.32×10^{-31}	CS: 2.28×10^{-4}	Classical velocity fine-tunes rapidly once the swarm approaches the feasible optimum.
f_7	Trid	0	CS: 7.90×10^{-10}	The baseline already obtains exact convergence in the reported trials.
f_8	Booth	7.76×10^{-28}	CS: 1.11×10^{-6}	The constrained minimum is easy for IPSO, so additional nonlocal sampling is less beneficial.
f_9	Matyas	1.96×10^{-35}	CS: 1.56×10^{-11}	The smooth landscape allows IPSO to exploit the optimum very accurately.
f_{10}	Liarwhd	8.87×10^{-32}	CS: 2.79×10^{-7}	IPSO already reaches the optimum; quantum movement mainly adds exploratory spread.

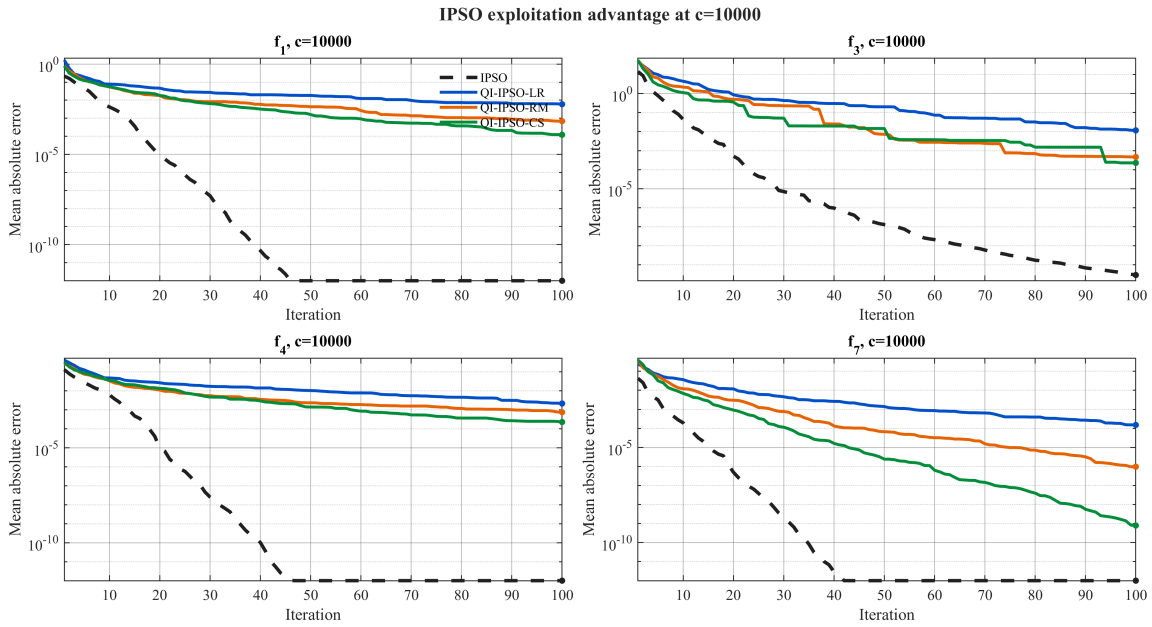

Figure 9: IPSO-favourable convergence curves for f_1, f_3, f_4, and f_7 at $c = 10000$, as summarized in Table 3.

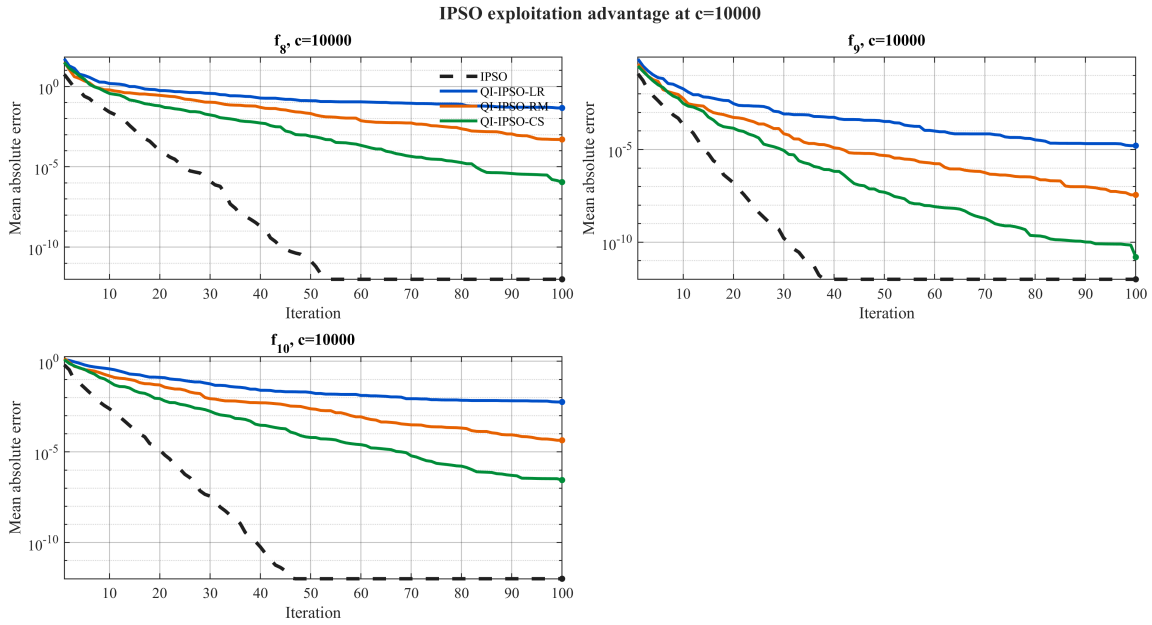

Figure 10: IPSO-favourable convergence curves for f_8, f_9, and f_{10} at $c = 10000$, as summarized in Table 3.

which the best QI-PSO variant improves MAE over IPSO; these are selective improvements rather than a majority of the full suite, and all eleven occur for the Rastrigin, Himmelblau, and Griewank functions. Among these improving cases, QI-PSO-CS is most frequently selected as the best quantum variant, QI-PSO-RM is best for several Griewank cases, and QI-PSO-LR is best for the most heavily penalized Rastrigin case. Together with the feasibility-rate columns, this supports the central claim that quantum displacement improves exploratory coverage and convergence in selected plateau-prone constrained multimodal landscapes while making the feasibility trade-off explicit.

Figures 5, 6, and 7 provide the corresponding convergence evidence. For f_2, f_5, and f_6, the multimodal structure creates repeated local attraction zones. In the Himmelblau case, Fig. 6 shows the improving penalty constants $c = 10$, 100, and 10000; the $c = 1000$ case is not plotted because IPSO already reaches essentially zero MAE at that penalty value and therefore is not an improving case in Table 2. The quantum displacement laws maintain nonlocal sampling around the attractor, giving the swarm more chances to leave a locally exploited basin; the retained attractor structure then continues to provide exploitation toward promising memory points. This behaviour is especially visible when the IPSO curve flattens while one of the QI-PSO variants continues to reduce the gap.

Table 3 and Figs. 9–10 provide the complementary evidence. In these cases, the baseline IPSO is better because the problem is already suitable for classical velocity-based exploitation: the known optimum is reached to machine precision or near-machine precision. This does not weaken the proposed method. Instead, it clarifies its role. QI-PSO is not proposed as a universal replacement for IPSO on every constrained function; it is a nonlocal search variant that is more attractive when the baseline shows plateau behaviour. In the full $c = 10000$ suite, the improvement is concentrated on f_2, f_5, and f_6; for the remaining functions, the baseline has already converged to machine precision and therefore leaves little room for improvement.

Generalization on Standard Benchmark Functions

The ten constrained benchmark functions from the study of Prajapati et al. [1] remain the primary test setting because they directly match the objective of this paper: testing nonlocal quantum-inspired movement in penalty-based constrained NLPPs. To examine whether the same movement mechanism has broader optimization value, an additional standard-benchmark evaluation was conducted using the baseline IPSO update and the three QI-PSO variants on selected unconstrained benchmark functions [16, 15]. Table 4 includes functions for which at least one QI-PSO variant produced a smaller mean-objective error than IPSO. These standard functions have distinct benchmark names from the ten constrained functions in Table 1, so the evaluation extends the numerical evidence without duplicating the original constrained test set. This subsection is therefore a supplementary selected-case check, not a claim of majority dominance over a full standard-function catalogue.

For this generalization evaluation, a case means one algorithm–function pair. Each such pair used 30 independent replications, population size 50, and 1000 iterations. The standard-benchmark runs used master seed 4040 with run seed $4040 + 100000\,\kappa_f + 1000\,\kappa_a + \ell$, using the same function, algorithm, and replication label convention as above. The reported error is

$$\mathcal{E} = \left| f_{\min} - \overline{f}_{\text{best}} \right|,$$

where $\overline{f}_{\text{best}}$ is the mean best objective value over the 30 trials and $f_{\min}$ is the reference optimum listed in the table. In Table 4, $x = (x_1, \ldots, x_n)$ is the decision vector for the listed dimension n, e is Euler's number, and the symbols a_{ij}, a_i, b_i, and c_i in the fixed-dimension benchmark formulas denote the standard tabulated benchmark constants from the cited sources, not algorithmic parameters. Table 4 is organized in a compact benchmark-reporting style consistent

with the rest of the manuscript: the function name, mathematical expression, domain, reference optimum, and corresponding IPSO-to-best-QI-PSO error comparison are placed together for direct comparison.

Table 4: Standard benchmark functions, domains, optima, and IPSO-to-QI-PSO error reductions. In the error column, LR, RM, and CS denote the Lorentz, Rosen–Morse, and Coulomb-like square-root potential-field variants, respectively.

Function	**Expression**	**Domain**	$f_{\min}$	**IPSO to best QI-PSO error**
Unimodal functions				
Sphere	$f(x) = \sum_{i=1}^{n} x_i^2$	$[-100, 100]$, $n = 30$	0	$6.5024\times10^{2} \rightarrow$ CS: 2.2414×10^{-1}; 99.97%
Schwefel No. 2.22	$f(x) = \sum_{i=1}^{n} \lvert x_i \rvert + \prod_{i=1}^{n} \lvert x_i \rvert$	$[-10, 10]$, $n = 30$	0	$1.5287\times10^{1} \rightarrow$ CS: 2.2341×10^{-2}; 99.85%
Step	$f(x) = \sum_{i=1}^{n} \lfloor x_i + 0.5 \rfloor^2$	$[-100, 100]$, $n = 30$	0	$7.8640\times10^{2} \rightarrow$ CS: 2.3333×10^{-1}; 99.97%
Multimodal functions				
Ackley	$f(x) = -20e^{-0.2\sqrt{\frac{1}{n}\sum_{i=1}^{n} x_i^2}} - e^{\frac{1}{n}\sum_{i=1}^{n}\cos(2\pi x_i)} + 20 + e$	$[-32, 32]$, $n = 30$	0	8.0785 $\rightarrow$ CS: 1.3959×10^{-1}; 98.27%
Fixed-dimension multimodal functions				
Shekel Foxholes	$f(x) = \left(\frac{1}{500} + \sum_{j=1}^{25} \frac{1}{j + \sum_{i=1}^{2} (x_i - a_{ij})^6} \right)^{-1}$	$[-65, 65]^2$	1	3.0765 $\rightarrow$ LR: 1.9952×10^{-3}; 99.94%
Kowalik	$f(x) = \sum_{i=1}^{11} \left(a_i - \frac{x_1(b_i^2 + b_i x_2)}{b_i^2 + b_i x_3 + x_4} \right)^2$	$[-5, 5]^4$	$3.075\cdot10^{-4}$	$3.1060\times10^{-2} \rightarrow$ RM: 4.7874×10^{-3}; 84.59%
Branin RCOS No. 1	$f(x) = \left(x_2 - \frac{5.1x_1^2}{4\pi^2} + \frac{5x_1}{\pi} - 6 \right)^2 + 10\left(1 - \frac{1}{8\pi}\right)\cos x_1 + 10$	$[-5, 15]^2$	0.398	$1.1264\times10^{-4} \rightarrow$ RM: 2.6624×10^{-5}; 76.36%
Shekel No. 7	$f(x) = -\sum_{i=1}^{7} \frac{1}{\sum_{j=1}^{4}(x_j - a_{ij})^2 + c_i}$	$[0, 10]^4$	-10.4028	3.6177 $\rightarrow$ LR: 8.3088×10^{-1}; 77.03%
Shekel No. 10	$f(x) = -\sum_{i=1}^{10} \frac{1}{\sum_{j=1}^{4}(x_j - a_{ij})^2 + c_i}$	$[0, 10]^4$	-10.5363	4.6332 $\rightarrow$ LR: 3.2178×10^{-1}; 93.05%

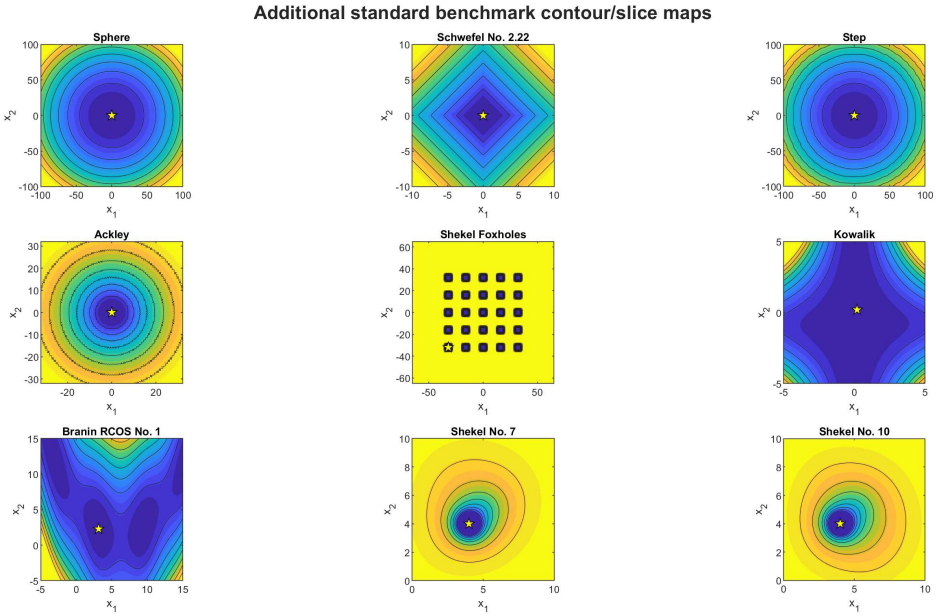

Figure 11: Contour and slice maps for the standard benchmark functions in Table 4; stars mark plotted optima.

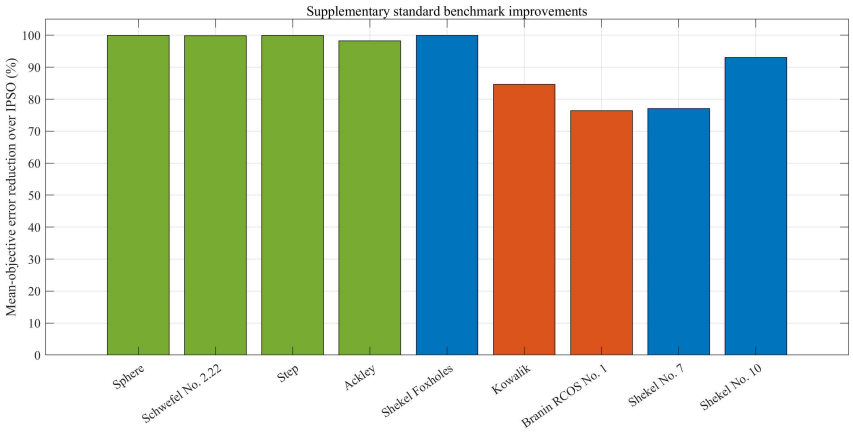

Figure 12: Error reduction for the standard benchmark functions in Table 4; bars show the best QI-PSO improvement over IPSO.

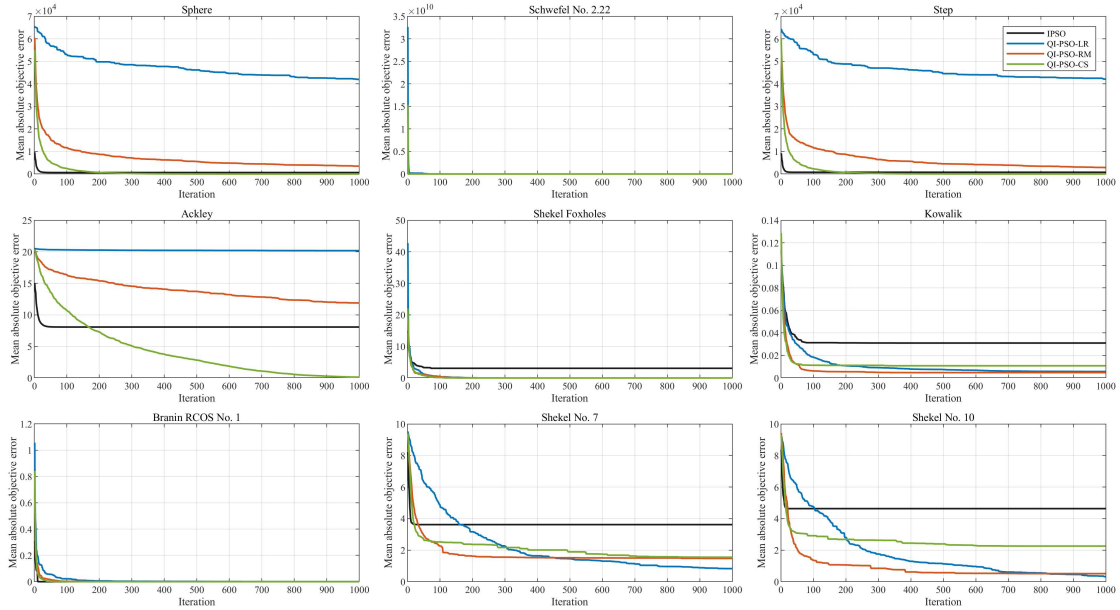

Figure 13: Mean convergence profiles for the standard benchmark functions in Table 4; curves show mean absolute objective error over 30 trials.

The standard benchmark results in Table 4 and Figs. 11–13 extend the same nonlocal-search argument developed from the constrained study. Table 4 reports nine non-overlapping standard functions for which at least one QI-PSO variant improves on IPSO. QI-PSO-CS is most effective on several high-dimensional landscapes, including Sphere, Schwefel No. 2.22, Step, and Ackley, where the IPSO search can remain far from the global optimum after repeated trials. QI-PSO-LR and QI-PSO-RM are more useful on some fixed-dimensional multimodal functions, such as Shekel and Kowalik cases, where occasional longer or differently shaped potential-induced moves help the swarm sample outside locally attractive regions. These results strengthen the interpretation that bounded-potential movement can improve IPSO when the search landscape benefits from stronger exploratory reach without discarding attractor-based exploitation, while the constrained suite remains the main problem setting of the manuscript.

7 Conclusion

This study proposed QI-PSO, a bounded-potential quantum-inspired variant of penalty-based IPSO for constrained NLPPs. The method keeps the quadratic penalty formulation and IPSO attractor structure, but replaces velocity-driven motion with quantum displacement. The one-step nonlocal-sampling analysis shows that, under local clustering, classical IPSO has a bounded damped step, whereas QI-PSO preserves a nonzero probability of moving outside a finite attractor neighbourhood. This explains its stronger ability to leave local attraction zones on selected plateau-prone multimodal landscapes while still exploiting personal and global best information through the attractor.

Numerically, the constrained improvement is selective: by MAE, the best QI-PSO variant improves 11 of the 40 function–penalty cases, consisting of four Rastrigin cases, three Himmelblau cases, and four Griewank cases. In those cases, the IPSO mean absolute error is reduced by 42.24% to 99.96%, with feasible-trial rates reported separately because some Rastrigin and Griewank improvements trade lower objective error for lower strict-feasibility frequency. The standard-benchmark generalization evaluation adds the nine improving unconstrained benchmark cases listed in Table 4, with reductions of 76.36% to 99.97% in the reported mean-objective error. The baseline IPSO remains preferable on exploitation-dominant constrained functions where it already reaches the known feasible optimum. Thus, QI-PSO is best viewed as a controlled exploratory variant for difficult multimodal landscapes, not as a universal replacement for velocity-based IPSO. Future work may consider higher-dimensional constrained benchmarks, adaptive potential selection, feasibility-prioritized selection rules, and hybrid IPSO–QI-PSO switching strategies.

Acknowledgements

The authors acknowledge the academic support and research environment that helped in the preparation of this manuscript.

Statements and Declarations

Funding

The authors declare that no funds, grants, or other support were received during the preparation of this manuscript.

Competing Interests

The authors have no relevant financial or non-financial interests to disclose.

Author Contributions

The first author, Prashant Kumar Pandey, contributed to conceptualization, numerical experimentation, and manuscript editing. The second author, Raju Prajapati, contributed to manuscript revision, methodological refinement, and interpretation of results. Both authors read and approved the final manuscript.

Data Availability

The datasets generated and analysed during the current study are available from the corresponding author on reasonable request.

Ethics Approval

Not applicable. This study did not involve human participants or animals.

References

[1] Prajapati R, Pal J, Dubey OP (2025) Measuring the role of penalty constant on nonlinear programming problem through computational experiments on benchmark functions. Int J Math Model Numer Optim 15(2):119–136

[2] Alvarez-Alvarado MS, Alban-Chacon FE, Lamilla-Rubio EA, Rodriguez-Gallegos CD, Velasquez W (2021) Three novel quantum-inspired swarm optimization algorithms using different bounded potential fields. Sci Rep 11:11655. https://doi.org/10.1038/s41598-021-90847-7

[3] Kennedy J, Eberhart R (1995) Particle swarm optimization. In: Proceedings of ICNN'95—International Conference on Neural Networks, vol 4. IEEE, Perth, pp 1942–1948. https://doi.org/10.1109/ICNN.1995.488968

[4] Poli R, Kennedy J, Blackwell T (2007) Particle swarm optimization: an overview. Swarm Intell 1(1):33–57. https://doi.org/10.1007/s11721-007-0002-0

[5] Shi Y, Eberhart R (2000) Comparing inertia weights and constriction factors in particle swarm optimization. In: Proceedings of the 2000 Congress on Evolutionary Computation. IEEE, La Jolla, pp 84–88. https://doi.org/10.1109/CEC.2000.870279

[6] Clerc M, Kennedy J (2002) The particle swarm—explosion, stability, and convergence in a multidimensional complex space. IEEE Trans Evol Comput 6(1):58–73. https://doi.org/10.1109/4235.985692

[7] Coello Coello CA (2002) Theoretical and numerical constraint-handling techniques used with evolutionary algorithms: a survey of the state of the art. Comput Methods Appl Mech Eng 191(11–12):1245–1287. https://doi.org/10.1016/S0045-7825(01)00323-1

[8] Mezura-Montes E, Coello Coello CA (2011) Constraint-handling in nature-inspired numerical optimization: past, present and future. Swarm Evol Comput 1(4):173–194. https://doi.org/10.1016/j.swevo.2011.10.001

[9] Parsopoulos KE, Vrahatis MN (2002) Particle swarm optimization method for constrained optimization problems. In: Sincak P, Vascak J, Kvasnicka V, Pospichal J (eds) Intelligent technologies—theory and applications: new trends in intelligent technologies. IOS Press, Amsterdam, pp 214–220

[10] Sun J, Feng B, Xu W (2004) Particle swarm optimization with particles having quantum behavior. In: Proceedings of the 2004 Congress on Evolutionary Computation. IEEE, Portland, pp 325–331. https://doi.org/10.1109/CEC.2004.1330875

[11] Sun J, Xu W, Feng B (2004) A global search strategy of quantum-behaved particle swarm optimization. In: Proceedings of the 2004 IEEE Conference on Cybernetics and Intelligent Systems, vol 1. IEEE, Singapore, pp 111–116. https://doi.org/10.1109/ICCIS.2004.1460396

[12] Sun J, Fang W, Wu X, Palade V, Xu W (2012) Quantum-behaved particle swarm optimization: analysis of individual particle behavior and parameter selection. Evol Comput 20(3):349–393. https://doi.org/10.1162/EVCO_a_00049

[13] Sun J, Liu J, Xu W (2007) Using quantum-behaved particle swarm optimization algorithm to solve non-linear programming problems. Int J Comput Math 84(2):261–272. https://doi.org/10.1080/00207160601170254

[14] Griffiths DJ, Schroeter DF (2018) Introduction to quantum mechanics, 3rd edn. Cambridge University Press, Cambridge

[15] Yang XS (2010) Engineering optimization: an introduction with metaheuristic applications. Wiley, Hoboken

[16] Andrei N (2008) An unconstrained optimization test functions collection. Adv Model Optim 10(1):147–161